Physica Scripta. Vol. T18, 111–118, 1987.

The Plasmapause Formation

J. Lemaire

Institut d'Aéronomie Spatiale de Belgique, 3, avenue Circulaire, B-1180 Bruxelles, Belgium

Received December 15, 1986; accepted December 30, 1986

Abstract

Convection velocities in the equatorial region of the magnetosphere have a large dawn–dusk asymmetry as well as a significant day–night asymmetry. The latter is the consequence of (i) day–night asymmetry of the ionospheric integrated conductivities and (ii) enhanced solar wind induced convection velocity in the midnight local time sector.

The observations indicate that the dynamics and the shape of the plasmasphere depend on geomagnetic activity as for instance measured by the K_p index. At each enhancement of K_p a new plasmapause density gradient is formed closer to the Earth in the nightside local time sector; this new density gradient corotates subsequently into the dayside local sector. Experimental evidence of peeling off of the nightside plasmasphere and of subsequent flux tube refilling processes is presented.

It is described how plasma interchange motion driven by the centrifugal force detaches plasma blocks from the gravitationally bound central part of the plasmasphere. At each new enhancement of the magnetospheric convection velocity in the midnight sector, the Zero Radial Force surface (i.e., where the radial component of the centrifugal force balances the gravitational force) penetrates deeper into the plasmasphere. The portion of plasmasphere beyond this critical surface is Rayleigh–Taylor unstable; this plasma shell is then detached with a velocity of interchange whose maximum value is determined by the value of the integrated Pedersen conductivity, Σ_p.

The kinetic theory for plasma interchange motion in the gravitational field is presented. The limiting effect of the ionospheric integrated Pedersen conductivity on interchange velocity is discussed. Plasma interchange motion driven by grad-B and curvature drift for plasma of non-zero temperature and anisotropic pitch angle distribution is also considered as an additional factor destabilizing the outer plasmasphere.

A review and critical analysis of the former "ideal MHD theory" for the formation of the plasmapause has been added.

1. Introduction

The plasmasphere is a ring-shaped region deep inside the magnetosphere, encircling the Earth around the Equator like a doughnut. It is filled with plasma of ionospheric origin. It contains therefore very low energy particles whose energies range between 0 and 1 eV. But more recently, suprathermal ions with an energy exceeding 10 eV have also been observed [1]. Unlike the very low energy plasma, the suprathermal particles have often an anisotropic pitch angle distribution.

2. Magnetospheric electric fields in the inner magnetosphere

As a result of field-aligned coupling the corotation electric field in the low altitude ionosphere maps up into the magnetosphere and forces the cold plasma trapped in the plasmasphere to corotate with the angular velocity of the Earth. Corotation is observed along all field lines whose McIlwain parameter (L) is smaller than 3 or 4, at least when the geomagnetic activity index K_p is smaller than 2. However, significant departure from corotation exists in the outer magnetosphere beyond $L = 4$ and especially when $K_p > 2$. The most characteristic departure from ideal corotation is consistently observed in the post-midnight sector where large azimuthal convection velocities in the eastward direction are constantly reported [2, 3, 40–42]; as a consequence, in this local time sector, the angular convection velocity is larger than the angular velocity of the Earth, as illustrated in Figs. 1(a) and 1(b).

Figure 1(a) shows the velocity vectors with which zero-energy plasma is convected around the Earth in the equatorial plane of the magnetosphere. In Fig. 1(b), the corotation velocity has been subtracted. It can be seen that in the post-midnight local time sector, a large eastward electric drift gives super-rotation of the magnetospheric plasma, while in the dayside part of the magnetosphere the local angular velocity is slightly smaller than the angular velocity of the Earth. These velocities vectors have been determined by using McIlwain's [3] non-axially symmetric magnetic field distribution (M2) and his electric field model distribution (E3H).

These empirical magnetic and electric field distributions have been determined from observations at geosynchronous orbit made with the spacecraft ATS 5. For relatively low geomagnetic activity conditions (i.e., for K_p between 1 and 2) this model is satisfactorily supported by independent observations from ATS 6 [27] and from other spacecraft like GEOS2.

However, when K_p increases, the geoelectric field becomes increasingly disturbed and non-stationary so that it is difficult to determine, under disturbed conditions, a standard electric field distribution in terms of stationary equipotential surfaces [4, 28].

In addition to the earthward drifts consistently observed in the midnight local time sector at the onset of substorm activity the eastward super-rotation convection velocity is then generally drastically enhanced and penetrates deeper into the plasmasphere. The dawn–dusk component of the electric field is then also significantly enhanced. All these features are, at least qualitatively, built in the E3H electric field [3] as well in the empirical model E5D recently presented by McIlwain [43].

3. The noon–midnight and dawn–dusk asymmetries

The enhancement of the dawn–dusk component of $\boldsymbol{E}$ at the onset of substorms gives rise to sunward motion of the plasma trapped along all geomagnetic field lines in the plasmasphere. As a consequence, in the nightside region, the plasmasphere is pushed toward the Earth and compressed. This gives rise to a general enhancement of the ambient plasma density. On the contrary, in the dayside local time sector, the equatorial plasma density decreases as a result of the sunward expansion of the plasmasphere, in response to a sudden enhancement of the dawn–dusk component of the geoelectric field distribution.

Another consistent feature, well represented in the electric field model E3H, is the observed noon-midnight asym-

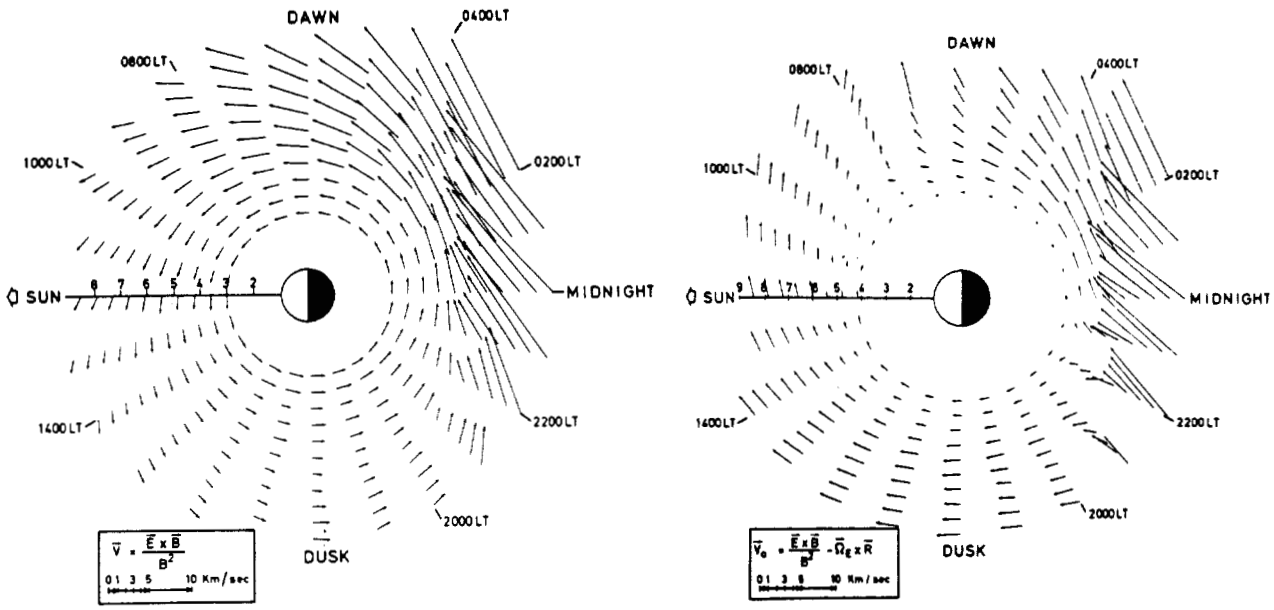

Fig. 1. Equatorial convection velocities corresponding to the electric and magnetic field models E3H and M2 (a) in the magnetospheric frame of reference, (b) in a corotation frame of reference. Note the change in the azimuthal velocity component, respectively, at 2230 LT and 0830 LT. (After Ref. [23].)

metry of the equipotential distribution. This noon–midnight asymmetry also shown in Figs. 1(a) and (b) has not only been observed in the ATS 5 observations [3] but also with PROGNOZ [5]. Whistler observations by Carpenter and Seely [6] shown in Fig. 2 also clearly indicate that under quiet geomagnetic conditions there is definitely a well developed noon–midnight asymmetry in the drift path of whistler ducts at all L-values in the plasmasphere. This noon–midnight asymmetry is also modelled in the low and mid-latitude electric field model deduced by Richmond [7] from radar observations.

Any theoretical electric field distribution like for instance the uniform dawn–dusk model [32–34] or the Volland–Stern [44, 45] model, which does not have this noon–midnight assymetry cannot be considered as a very realistic representation of the actual geoelectric field distribution in the magnetosphere. Indeed, the integrated Pedersen and Hall conductivities in the ionosphere are always strongly asymmetric with respect to the dawn–dusk meridian; as a consequence of this persistend day–night asymmetry of the ionospheric electric conductivity, the magnetospheric electric field must necessarily have a similar persistent day–night asymmetry.

When K_p decreases corotation extends to larger radial distances in the magnetosphere; the dawn–dusk asymmetry of the magnetospheric convection flow pattern is then significantly reduced [4, 6, 7].

4. Plasma density distribution in the plasmasphere

The thermal plasma within the plasmasphere is trapped along geomagnetic field lines, and confined close to the Earth by the gravitational field. In the topside ionosphere, the plasma density decreases exponentially as a function of altitude with a characteristic scale height which is inversely proportional to

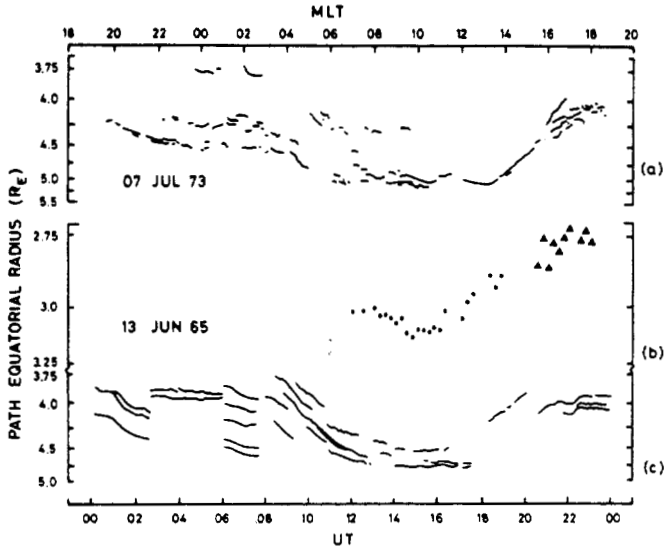

Fig. 2. Variation of whistler equatorial radius with time during two exceptionally quiet 24-h periods. The equatorial radius of whistler paths are plotted as a function of magnetic local time at the observing whistler station. Each sequence represents a particular whistler path (after Ref. [6]).

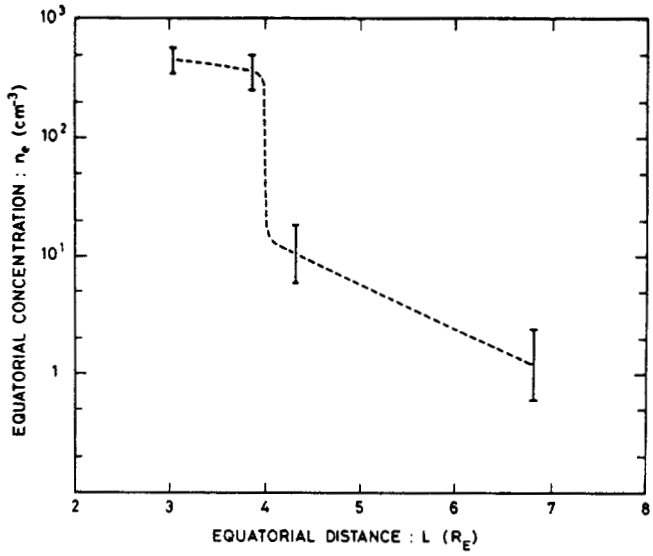

Fig. 3. Equatorial electron density distribution as determined from whistler observations (after Ref. [8]).

the gravitational force (mg). At an altitude of 1000 km the plasma density is a few thousand particle/cm^3. Since the gravitational force decreases as r^{-2}, the density scale height increases, and, the slope of the equatorial density distribution slowly decreases as altitude increases. At an equatorial distance of 4 Earth radii ($L = 4$) the equatorial plasma density is reduced to a value of the order of 300 cm^{-3} or 500 cm^{-3} (see Fig. 3).

Carpenter [8] discovered from whistler observations in 1963 that this monotonic decrease of the plasma density in the gravitational field is generally interrupted by a sharp "knee" at a radial distance varying between 4 and 6 Earth radii. At this distance the equatorial electron density decreases sometimes very abruptly by two orders of magnitude over a rather short radial distance (0.15 R_E). The region where this sharp density gradient was observed from ground based whistler observations [8] and from in-situ satellite measurements [9, 10], is called the *plasmapause*; the plasmapause "knee' forms the outer edge of the plasmasphere.

5. Plasmapause positions in the nightside sector

In 1966, Carpenter [11] investigated the local time dependence of the plasmapause surface. The solid line in Fig. 4 gives the average shape of the equatorial cross section of the plasmasphere under steady, moderate activity conditions (K_p = 2–4). The dawn–dusk asymmetry of the plasmasphere is clearly identified by the existence of a bulge near 1800 Local Time.

The dotted line in Fig. 4 gives the positions of the plasma pause "knee" during a period of increasing geomagnetic activity. On the contrary, the dashed line corresponds to the observed plasmapause positions for a period of decreasing geomagnetic activity. These observations indicate that the shape of the plasmasphere and of its outer boundary depend strongly on K_p and on the evolution of this geomagnetic index during the 24 h preceding the observation.

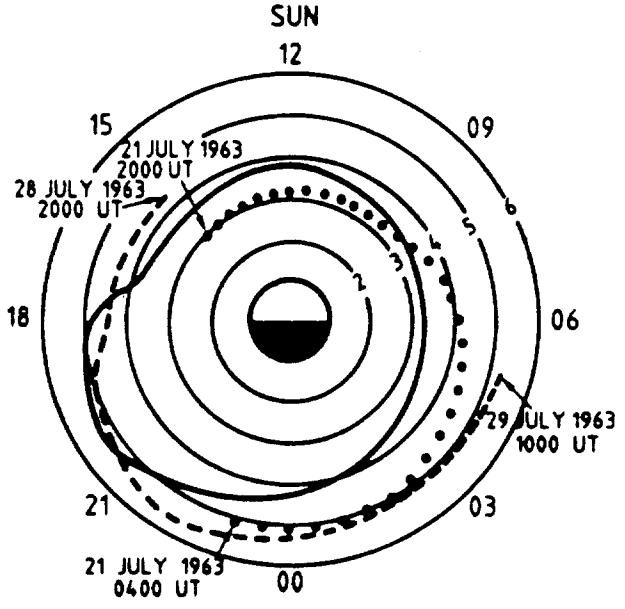

Fig. 4. Equatorial radius of the plasmapause vs. local time. The solid line represents average behavior during periods of moderate, steady geomagnetic agitation (K_p = 2–4). The observations were made in July and August 1963 at Eights, Antarcita. The dots show a particular example involving increasing magnetic agitation; the dashes, correspond to a period of decreasing agitation (after Ref. [11]).

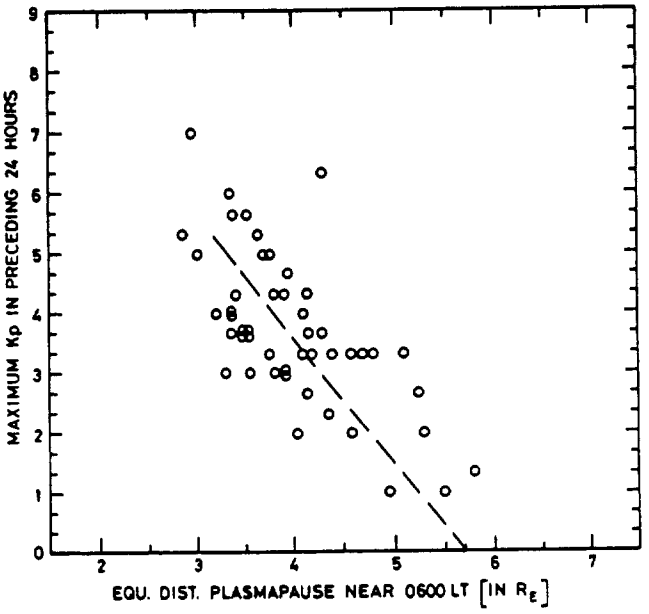

Fig. 5. Relation between the dawn minimum in the equatorial radius of the plasmapause and maximum value of K_p during the 24 h preceding the observation at Byrd station (after Ref. [31]). The dashed line corresponds to the average positions of the post–midnight plasmapause position as a function of the maximum value of K_p during the 12 h preceding the observations (after Ref. [12]).

This is also illustrated in Fig. 5 where the dots represent the observed position of the plasmapause in the nightside sector as a function of the maximum value of K_p during the 24 h preceding the observation [31]. This scatter diagram clearly indicates a negative correlation between the plasmapause position (L_{pp}) and the geomagnetic activity index. The dashed line in Fig. 5 is a regression line between the post-midnight plasmapause position and the maximum value of the K_p index during the 12 hours preceding the whistler observations [12]. For instance, when $K_p = 0$, $L_{pp} = 5.7$; for $K_p = 5$, $L_{pp} = 3.35$. Similar results have been reported in Refs. [35] and [36].

All available observations confirm that the position of the plasma density knee (i.e., the plasmapause) in the post-midnight local time sector responds almost immediately to a rapid enhancement of K_p [12, 30]. At each such enhancement of geomagnetic activity a new density gradient is formed closer to the Earth as a direct response to the enhanced convection velocity in the midnight sector. This is clear evidence that the plasmapause is generally formed in the nightside local time sector where the convection velocity is largest.

6. Plasmapause positions in the dayside local time sector

In the dayside local time sector, the plasmapause position is closer to the Earth only later on, i.e., with a time delay corresponding to the time needed for the new density gradient formed in the night sector to corotate into the dayside sector [13, 14]. It appears therefore that the night local time sector is the region where the plasmapause is formed, i.e., where sharp density gradients are formed at each new enhancement of geomagnetic activity (Fig. 6).

7. A characteristic sequence of events

Figure 7 illustrates a sequence of cold ion density profiles as

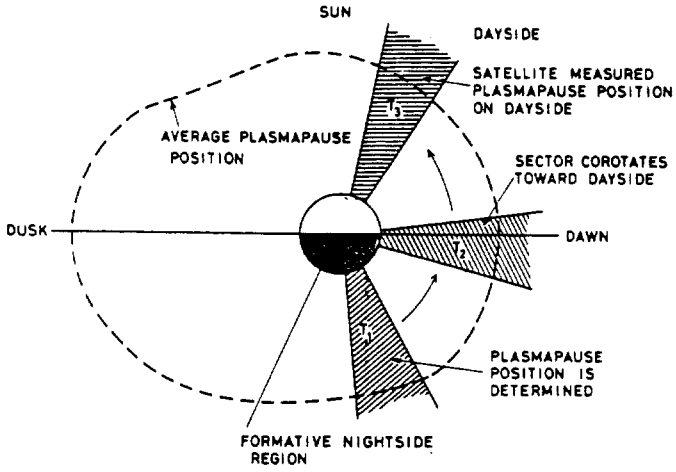

Fig. 6. Average plasmapause position as determined from cold ion density distributions measured along OGO 5 orbits. The formation of the plasmapause density gradient in the midnight local time sector is indicated in this figure at time T_1; the corotation of the new density knee in the dayside local time sector is illustrated at time T_2 and T_3 (after Ref. [13]).

determined along a series of OGO 5 orbits at different epochs during the development of an extended series of substorm [16]. At some arbitrary choosen time t_0 preceeding the large K_p enhancement, the equatorial plasma density in the post-midnight local time sector (MLT = 01–05), was assumed to be given by the L^{-4} curve extending up to L-values larger than 8. At time t_1, just after the large K_p enhancement, a very sharp density gradient has appeared along the field line $L = 3$ where it is expected for $K_p = 6^-$ according to Carpenter and Parks' [12] relationship (given by the dashed line in Fig. 5). At time t_2, it can be seen that flux tube refilling has already taken place and increases the ambient plasma density beyond $L = 3$.

Note that the equatorial density has increased more rapidly at lower L-values than at larger L-values. This differential flux tube refilling is a consequence of the increasing volume of flux tubes as a function of L. Indeed, it takes more time to refill a large flux tube than to refill a smaller one at lower L-values.

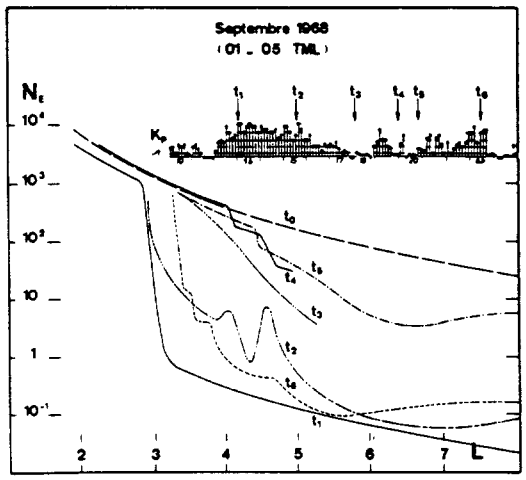

Fig. 7. The evolution of the equatorial plasma density distribution in the 0100–0500 MLT sector during a period of time of several days in September 1968. These distributions have been obtained from OGO 5 observations at different times $t_1, \ldots, t_6$ indicated on the Bartels diagram giving the geomagnetic index K_p during this extended period of time when significant substorm activity started on 12th September (after Ref. [16]).

At time t_3, when geomagnetic activity has been reduced to a rather low value, magnetic flux tubes beyond $L = 3$ are still in the process of refilling, but the equatorial density has increased by almost two orders of magnitude at $L = 4$. At time t_4, immediately after a series of short duration and lower amplitude K_p-enhancement, a new plasmapause is formed at $L = 4$; it can also be seen that there are a series of steps (multiple knees) in the equatorial density beyond the innermost density gradient.

At time t_5 refilling has taken place and a much smoother density profile is observed. A small gradient remains at $L = 4.5$. Finally, at t_6 in the middle of a new K_p-enhancement, a new density gradient has formed at $L = 3.4$ again with the formation of different plateaus resulting from a series of successive K_p-enhancements with decreasing amplitudes.

Note that all the density profiles shown in Fig. 7 have been obtained in the post-midnight local time sector between 0100 LT and 0500 LT. It is also worthwhile to point out in the density profile corresponding to time t_2, the presence of a detached plasma element beyond $L = 4.2$ a few hours after an enhancement of K_p; this plasma density enhancement is found beyond the location where the formation of a new plasmapause is expected when $K_p = 3$ according to Carpenter and Parks' relationship illustrated by the dashed line in Fig. 5.

8. Local time distribution of detached plasma elements

A large number of well detached plasma elements have been found in the after-noon local time sector using OGO 5 density profiles [17]. These detached plasma elements or plasma tails correspond to large density enhancements exceeding the arbitrary L^{-4} threshold (n_s) shown in Fig. 8. It is not absolutely clear, however, from Ref. [17] whether the larger *number* of detached plasma elements reported in the afternoon is indeed a true enhancement in the *actual frequency* distri-

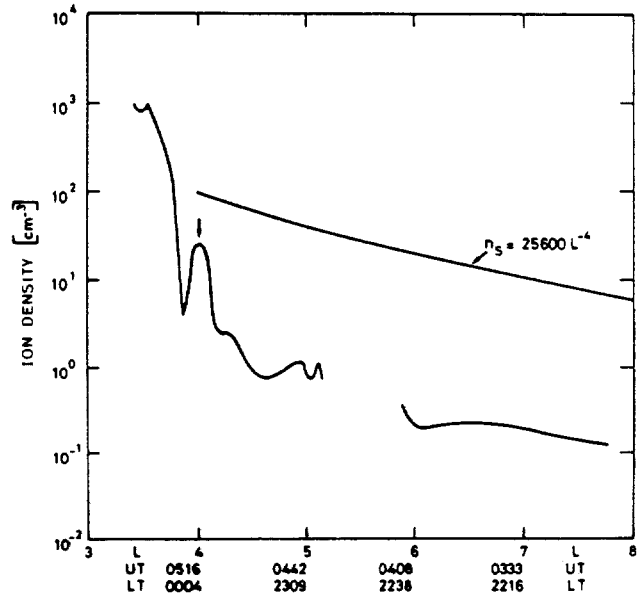

Fig. 8. Equatorial density of thermal ions observed in the magnetosphere along the trajectory of OGO 5 in the nightside local time sector. At $L = 4$ a plasma element is in the process of detachment (Courtesy NSSDC). The solid line (n_s) corresponds to a threshold density used in Ref. [17] to identify large amplitude density peaks corresponding to detached plasma elements (after Ref. [18]).

bution of detached plasma elements in the afternoon sector. Indeed a non uniform LT distribution of OGO 5 sample orbits combined with an arbitrary density threshold may possibly lead to biased results.

Instead of using an arbitrary threshold ($n_s = 25\,600\,L^{-4}$, see Fig. 8) to identify the presence of detached plasma elements beyond the plasmapause, Kowalkowsky and Lemaire [18] in a latter statistical study of the same OGO 5 measurements used a morphological criterium to identify the detached elements. For instance, the density enhancement at $L = 4.1$ (indicated by a vertical arrow in Fig. 8) has not been considered as a true plasma detachment and was not taken into account in the former study [17], since it does not cross the arbitrary density threshold curve (straight line in Fig. 8). On the contrary in the latter study [18], such a density enhancement has been considered as a detached plasma element, and it has been included in the frequency distribution deduced from the same OGO 5's equatorial plasma density measurements.

These additional plasma elements are not always fully detached nor do they always have a density peak exceeding the threshold value like the detached element illustrated in Fig. 8; these plasma density enhancements are generally observed after disturbed periods when K_p has been high during the 3 or 6 hours preceding the passage of the spacecraft in the post-midnight local time sector.

The statistical study [18] including plasma elements in process of detachment, like that one shown in Fig. 8, has indicated that the relative number of plasma detachments in the post-midnight sector for shifted $K_p < 2$, is much smaller than when $K_p > 2$. This statistical study confirms then the conclusions sketched in Fig. 6: (i) plasma detachment occurs also, if not exclusively, in the nightside sector and (ii) a new "knee" in the equatorial density distribution is formed there each time geomagnetic activity level is suddenly enhanced, i.e., each time the eastward convection velocity is increased in the midnight sector.

Although, the observational results reported in Refs. [17] and [18] are consistent with the physical theory reviewed in the following part of this article, a word of caution is needed, however, concerning the reliability of the OGO 5 measurements used in both studies. Indeed, because of spacecraft charging the densities of cold plasma deduced from OGO 5 light ion-mass spectrometer are now suspected to be in error by undetermined factors (Chappell, 1974, private communication, and Horwitz, 1986, private communication). Therefore, the conclusions drawn from OGO 5 cold plasma density measurements must be considered as questionable.

However, in the statistical study by Kowalkowski and Lemaire [18] precise absolute values for these density measurements were not required, only changes in the density gradients (slopes) were needed in Ref. [18] to identify the plasmapause and detached plasma elements. Therefore, assuming that the undetermined correction factors do not change drastically from one measurement to the next, there are good reasons to believe that most of the "knees" identified in OGO 5 density measurements (like in Figs. 7 or 8) are indeed real structures in the cold plasma density distributions.

Of course, an independent verification of the conclusions of Refs. [17] and [18], based on other spacecraft measurements devoid of such instrumental uncertainties would be required to clarify this issue. Anderson [37] has identified similar density knees and detached plasma elements at all local times (even in the midnight sector) using ISEE-1 wave experiment. But final results from this study are not yet available.

9. A physical mechanism for detaching plasma elements

The detachment of plasma elements from the plasmasphere is schematically illustrated in Fig. 9, as well as the physical mechanism leading to peeling of the plasmasphere. To comprehend this mechanism, it is useful to recall that the gravitational force determines the density scale height, in the whole ionosphere; i.e., that the negative density gradient characterizing the altitude distribution of cold plasma in the topside ionosphere and in the ion-exosphere is actually determined by the gravitational potential.

Any positive (reversed) plasma density gradient in the upper ionosphere would immediately trigger Rayleigh–Taylor instability; spontaneous plasma motions driven by this instability tend to restore a density distribution with a negative gradient at all altitudes – at least where the gravitational force dominates. Indeed, one cannot maintain in mechanical equilibrium a layer with an excess density (or a plasma irregularity) on top of a layer of lower density. Plasma interchange motion driven by the gravitational force moves the denser plasma cloud in the direction of the external force toward a place where the background plasma density is equal to the density of the plasma cloud itself. Therefore, all positive plasma density gradients in the upper ionosphere and in the inner magnetosphere, where the gravitational force is dominant, are unstable and lead to interchange motion. A detailed kinetic description of plasma interchange motion in the gravitational field has been presented in Ref. [23].

Since the plasmasphere corotates and even super-rotates in the night local time sector [see Fig. 1(a) and (b)], there is always a limit beyond which the gravitational force is balanced by the centrifugal force. Beyond that limit called the Zero Radial Force surface (ZRF), the external force acting on any cold plasma cloud (plasma density enhancement) is directed away from the Earth. Any such cloud of plasma located beyond the ZRF surface is forced by interchange to move away from Earth toward the magnetopause. In other words, any negative density gradient beyond the ZRF surface is Rayleigh–Taylor unstable and tends to detach from the

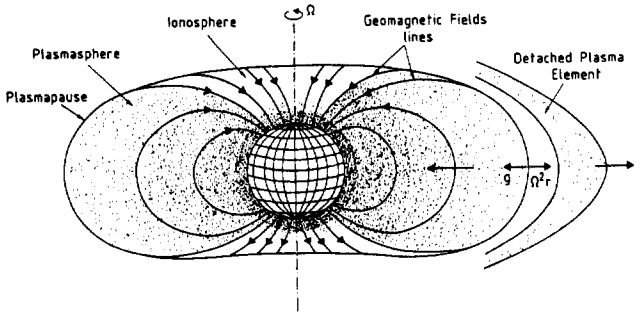

Fig. 9. Three-dimensional illustration of the plasmasphere and of its outer boundary: the plasmapause. Under enhanced magnetospheric convection events, blocks of plasma can detach in the night local time sector as a consequence of enhanced centrifugal effects. The electric resistivity of the lower ionosphere limits the growth rate of plasma interchange instability responsible for the plasma detachment and peeling off of the nightside plasmasphere.

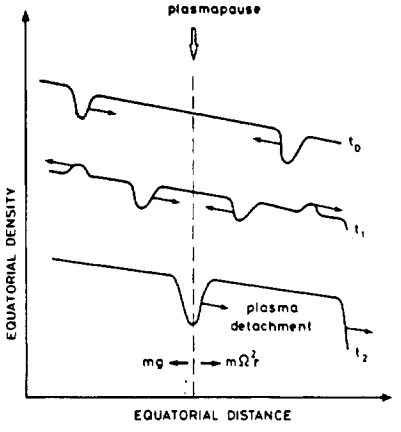

Fig. 10. Equatorial density distribution with two plasma holes drifting toward a common asymptotic trajectory determined by the balance between the mean gravitational force and the radial component of the centrifugal force. All plasma holes collect along this trajectory. As a consequence a trough is developing along the Zero Radial Force (ZRF) surface. The large plasma density enhancement formed beyond this trough drifts away from the main plasmasphere by interchange motion. Indeed, beyond the dashed line corresponding to the ZRF surface the centrifugal force exceeds the gravitational force. A sharp "knee" in the equatorial density remains when the block of plasma has separated from the central part of plasmasphere which is trapped within the gravitational potential well. This figure illustrates how a new plasmapause density gradient is formed by peeling off a shell of the plasmasphere via interchange motion (after Ref. [23]).

innermost part of the plasmasphere which is located inside this surface. A different way to describe this physical mechanism is illustrated in Fig. 10.

Superimposed on the equatorial density profiles shown in Fig. 10, there are a series of plasma density holes (density depletions). The plasma density holes located inside the ZRF surface move upwards like bubbles in the gravitational field. On the other hand, the plasma holes which are located beyond the ZRF surface move toward the Earth until they reach the ZRF surface where all such plasma holes converge. This forms a trough at the location of the ZRF surface where the gravitational and the radial component of centrifugal force balance each other. The plasma with a negative density gradient extending beyond the ZRF surface is Rayleigh–Taylor unstable; this block of plasma is therefore forced to move outwards under the action of the pseudo-centrifugal force; this finite shell of dense plasma gets then detached from the plasmasphere like an iceberg from the icebank.

10. The growth rate of interchange instability

In the framework of infinitely conducting fluids (i.e., ideal MHD) such a detachment would not be possible; indeed, the plasma interchange velocity becomes vanishingly small when the perpendicular conductivity has an infinitely large value somewhere along the magnetic field lines.

But the magnetosphere and ionosphere is not an ideal MHD system. The integrated Pedersen conductivity along geomagnetic field lines is not infinitely large nor is it equal to zero. As a consequence the maximum plasma interchange velocity, which is inversely proportional to the integrated Pedersen conductivity [23], is not equal to zero, nor is it arbitrarily large as implicitly assumed in earlier studies of interchange instabilities [19–22, 38].

It is the value of the integrated Pedersen conductivity which determines the rate at which the gravitational or centrifugal potential energy can be dissipated by Joule heating in the E-region of the ionosphere. A value of 1 Siemens for the integrated Pedersen conductivity leads to a maximum plasma interchange velocity of the order of about 10% of the large scale magnetospheric convection velocity illustrated in Fig. 1. Although this interchange velocity is a relatively small fraction of the overall corotation-convection velocity, it is however a key element in the process of detachment of plasma elements.

It is in the night sector that the integrated Pedersen conductivity is smallest, and, consequently it is there that the interchange velocity can obtain the highest maximum values.

It is also in the nightside that the convection velocity is largest and that the ZRF surface penetrates deepest into the magnetosphere (see Ref. [23]). Consequently it is there that interchange motion driven by the centrifugal force is most effective in peeling off the plasmasphere.

11. Formation of new density knees at each new enhancement in magnetospheric convection

New plasma detachment and plasma density gradients are formed closer to the Earth each time when K_p is suddenly enhanced. Indeed, when K_p is enhanced, we have seen before that the magnetospheric convection velocity is also drastically enhanced. As a result of this enhancement of the eastward azimuthal velocity, the ZRF surface penetrates closer to the Earth in the whole nightside sector. The negative density gradient beyond the new position of this critical surface becomes unstable. The larger the K_p enhancement, the larger is the fraction of the plasmasphere which is peeled off.

Note that the ZRF extends in the pre-midnight sector. Consequently, one expects the formation of density gradients by interchange motion, even in the pre-midnight sector. The minimum radial distance of the ZRF surface when calculated using the E3H and M2 models, is located between 0100 and 0200 LT; but for other E-field models it may well be located in the pre-midnight local time sector.

12. Diamagnetic and finite temperature effects

The diamagnetic signatures expected at the surface of these cold plasma elements or at the plasmapause itself are small as a consequence of the small value of β, the ratio between the kinetic plasma pressure and magnetic pressure.

A more detailed discussion of the diamagnetic effect of plasma density irregularity is presented in Ref. [23]; it indicates that any excess kinetic pressure inside such detached plasma density irregularities, would immediately force the volume of this element to increase until the internal density and temperature are reduced by the appropriate factors to restore mechanical equilibrium: i.e., until total pressure is balanced across its surface [25].

Interchange motion resulting from gradient-B and from the centrifugal force on non-zero energy particles spiraling along curved magnetic field lines has also been considered in Ref. [23].

It is worthwhile to mention that the presence of a suprathermal component in the outer plasmasphere does not necessarily enhance or inhibit the interchange motion of cold plasma cloud or irregularities. Indeed, it is not the temperature difference but well the density difference between the

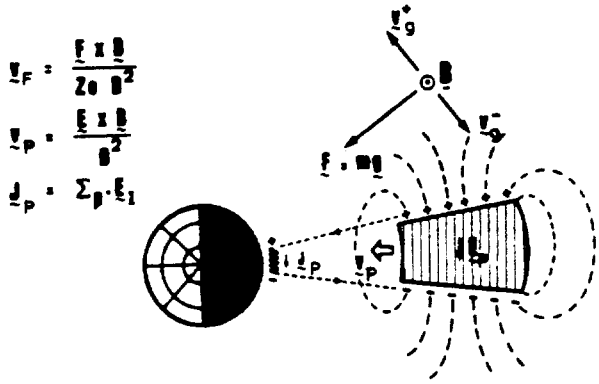

Fig. 11. Description of plasma interchange motion illustrating a cold plasma element falling across geomagnetic field lines with a maximum interchange velocity V_p in the gravitational field. The gravitational drifts of the ions and electrons give rise to a polarization electric field E_p. The resulting electric drift V_p is parallel to the gravitational force (after Ref. [23]).

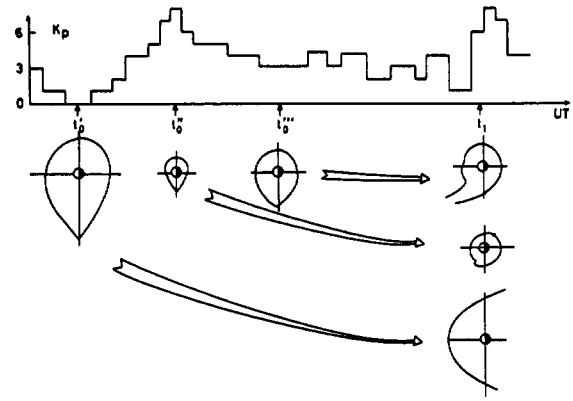

Fig. 12. The evolution of plasmapause positions identified with the last closed equipotential surfaces at three different initial times t_0', t_0'' and t_0'''. The positions of the plasmapause at the same t_1 depend on the arbitrary choice of t_0 the initial time for the numerical integration. For instance if t_0 is choosen at t_0', when K_p the geomagnetic index is equal to zero, the last closed equipotential drifts to the magnetopause in less than 36 h [46].

inside and outside which determines the buoyancy force of a hot air balloon and also of a hot plasma cloud.

Non-zero temperature effects become important for the interchange of hot plasma clouds when β is large and when the parallel and perpendicular kinetic pressures inside the plasma element are very different from those outside, i.e., when $\Delta p_\parallel$ and $\Delta p_\perp$ are of the order of $p_\perp$ and $p_\parallel$ respectively [23, 39].

A positive plasma temperature gradient like that observed in the plasmasphere increases the convective stability of the plasma gravitationally trapped below the Zero Radial Force surface; on the contrary this same temperature slope destabilizes the layers beyond the ZRF surface where $g_{\text{eff}} = 0$ [39].

Consequently, the positive temperature gradient observed in the outer part of the plasmasphere and beyond the plasmapause accentuates the key role of the ZRF surface and of plasma interchange motion in the theory of formation of the plasmapause. The observed temperature slope enhances the growth rate of the Rayleigh–Taylor instability without changing significantly the location where it is triggered (i.e., at the ZRF surface).

13. The ideal MHD theory for the formation of the plasmapause

In the former ideal MHD theory [29, 32] for the formation of the Plasmapause, it is considered that a sharp density gradient continuously forms at dusk, where the convection velocity is small (i.e., equal to zero); in other words, the peeling of the plasmasphere is expected to take place at the stagnation point where $\boldsymbol{E}$ and $\boldsymbol{E} \times \boldsymbol{B}/B^2$ are both equal to zero i.e., not in the midnight sector where these quantities have their largest values.

In this case, one would expect the sharpest density gradients to be formed in the dusk local time sector, immediately after each substorm onset. However, this does not seem to be the case, since the sharpest density knees are observed in the midnight local time sector.

Furthermore, the observed positions of the plasmapause in the dusk sector are much less well correlated with K_p than the plasmapause positions observed in the post-midnight local time sector. Consequently, it must be admitted that the dusk sector is not the most frequent nor the most likely site for the formation of sharp density gradients which are generally identified with the equatorial plasmapause.

Furthermore, the ideal MHD theory originally proposed for stationary models of the magnetic and electric field distributions, fails to give uniquely defined plasmapause positions for time dependent $\boldsymbol{E}$ and $\boldsymbol{B}$-models. This is illustrated in Fig. 12 where it is shown that plasmapause positions are not independent of the initial boundary conditions at $t = t_0$: i.e., at the initial time of numerical model integration. There is obviously a conceptual problem when the final answer (e.g., the plasmapause positions at a fixed time t_1) depends on t_0, the time arbitrarily choosen to start time dependent numerical simulations. This is therefore one additional reason to question ideal MHD theory for the formation of a plasmapause, when electric and magnetic field distributions are not time independent.

The alternative physical mechanism reviewed above does not suffer of these conceptual difficulties; it is not based on the existence of any mathematical singularity (i.e., a stagnation point where $\boldsymbol{E} = 0$) in the large scale magnetospheric electric field distribution; but this physical mechanism works as well whether or not one or more stagnation points exist in the E-field model assumed.

Acknowledgements

I wish to thank the "Fonds National de la Recherche Scientifique" and the "Ministère de l'Education Nationale" for financial support. I wish also to thank Y. Corcuff, C. R. Chappell, P. Decreau, and R. A. Wolf for their comments and for stimulating discussions with them.

References

1. Chappell, C. R., Green, J. L., Johnson, J. F. E., and Waite, J. H., Jr., Geophys. Res. lett. **9**, 933 (1982).
2. Axford, W. I. and Hines, C. O., Canad. J. Phys. **39**, 1433 (1961).
3. McIlwain, C. E., Substorm injection boundaries, Magnetospheric Physics, pp. 143–154 (Edited by B. M. McCormac), D. Reidel Publ. Co, Dordrecht, Holland (1974).
4. Baumjohann, W., Haerendel, G., and Melzner. F., J. Geophys. Res. **90**, 393 (1985).
5. Gringauz, K. I. and Bezrukih, V. V., J. Atmos. Terr. Phys. **38**, 1071 (1976).
6. Carpenter, D. L. and Seely, N. T., J. Geophys. Res. **81**, 2728 (1976).
7. Richmond, A. D., J. Geophys. Res. **81**, 1447 (1976).

8. Carpenter, D. L., J. Geophys. Res. **68**, 1675 (1963).
9. Gringauz, K. I., Kurt, V. G., Moroz, I., and Shklovskii, I. S., Soviet Astronomy-AJ **4**, 680 (1960).
10. Chappell, C. R., Harris, K. K., and Sharp, G. W., J. Geophys. Res. **75**, 50 (1970a).
11. Carpenter, D. L., J. Geophys. Res. **71**, 693 (1966).
12. Carpenter, D. L. and Park, C. G., Rev. Geophys. Space Phys. **11**, 133 (1973).
13. Chappell, C. R., Harris, K. K., and Sharp, G. W., J. Geophys. Res. **76**, 7632 (1971).
14. Decreau, P. M. E., Beghin, C., and Parrot, M., J. Geophys. Res. **87**, 695 (1982).
15. Higel, B. and Wu Lei, J. Geophys. Res. **89**, 1583 (1984).
16. Corcuff, P., Corcuff, Y., Carpenter, D. L., Chappell, C. R., Vigneron. J., and Kleimenova, N., Ann. Géophys. **28**, 679 (1972).
17. Chappell, C. R., J. Geophys. Res. **79**, 1861 (1974).
18. Kowalkowski, L. and Lemaire, J., Bull. Classe Sci., Acad. Royale Belgique **65**, 159 (1979).
19. Cheng, A. F., J. Geophys. Res. **90**, 9900 (1985).
20. Melrose, D. B., Planet. Space Sci. **15**, 381 (1967).
21. Gold, T., J. Geophys. Res. **64**, 1219 (1959).
22. Hill, T. W., Planet. Space Sci. **24**, 1151 (1976).
23. Lemaire, J., Frontiers of the plasmasphere, Thèse d'Agrégation de l'Enseignement Supérieur, UCL, Ed. CABAY, Louvain-la-Neuve; Aeronomica Acta A298 (1985).
24. Gringauz, K. I., Space Sci. Rev. **34**, 245 (1983).
25. Longmire, C. L., Elementary Plasma Physics, Interscience, New York (1963).
26. Bostick, W. H., Phys. Rev. **104**, 292 (1956).
27. Lemaire, J., Bull. Classe Sci., Acad. Royale de Belgique **68**, 821 (1982).
28. Pedersen, A., Cattell, C. A., Falthammar, C. -G., Formisano, V., Lindqvist, P. -A., Mozer, F., and Torbert, R., Quasistatic electric field measurements with spherical double probes on the GEOS and ISSE satellites, Space Sci. Rev. **37**, 269 (1984).
29. Brice, N. M., J. Geophys. Res. **72**, 5193 (1967).
30. Park, C. G., J. Geophys. Res. **75**, 4249 (1970)
31. Carpenter, D. L., J. Geophys. Res. **72**, 2969 (1967).
32. Kavanagh, L. D., Jr., Freeman, J. W., Jr. and Chen, A. J., J. Geophys. Res. **73**, 5511 (1968).
33. Grebowsky, J. M., J. Geophys. Res. **75**, 4329 (1970).
34. Chen, A. J. and Wolf, R. A., Planet. Space Sci. **20**, 483 (1972).
35. Rycroft, M. J. and Burnell, S. J., J. Geophys. Res. **75**, 5600 (1970).
36. Rycroft, M. J. and Thomas, J. O., Planet. Space Sci. **18**, 65 (1970).
37. Anderson, R. R., ISEE-1, Wave measurements of the plasmasphere shape, Presented at COSPAR Symposium No. 9, Toulouse (1986).
38. Sonnerup, B. U. O. and Laird, M. J., J. Geophys. Res. **68**, 131 (1963).
39. Lemaire, J., Plasma interchange motion in a non-ideal MHD; system (in preparation) (1987).
40. Foster, J. C., J. Geophys. Res. **88**, 981 (1983).
41. Alcayde, D., Caudal, G., and Fontanari, J., J. Geophys. Res. **91**, 233 (1986).
42. Greenwald, R. A., Space Science Reviews **34**, 305 (1983).
43. McIlwain, C. E., A K_p dependent equatorial electric field model, Presented at Cospar Symposium No. 9, Toulouse, July (1986).
44. Volland, H., Ann. Géophy. **31**, 159 (1975).
45. Stern, D. P., Rev. Geophys. Space Phys. **15**, 156 (1977).
46. Corcuff, Y., Corcuff, P., and Lemaire, J., Ann. Geophys. **3**, 569 (1985).